Analysis of Dynamic Cerebral Contrast–Enhanced Perfusion MRI Time–Series Based on Unsupervised Clustering Methods

Oliver Lange, Anke Meyer–Bäse,

Department of Electrical and Computer Engineering,
Florida State University, Tallahassee, Florida 32310-6046 USA

Axel Wismüller, and

Department of Clinical Radiology, Ludwig–Maximilians University,
Munich 80336, Germany

Monica Hurdal

Department of Mathematics,
Florida State University, Tallahassee, Florida 32306-4510 USA

ABSTRACT

We employ unsupervised clustering techniques for the analysis of dynamic contrast-enhanced perfusion MRI time-series in patients with and without stroke. "Neural gas" network, fuzzy clustering based on deterministic annealing, self-organizing maps, and fuzzy c-means clustering enable self-organized data-driven segmentation w.r.t. fine-grained differences of signal amplitude and dynamics, thus identifying asymmetries and local abnormalities of brain perfusion. We conclude that clustering is a useful extension to conventional perfusion parameter maps.

Keywords: Dynamic contrast–enhanced imaging, perfusion imaging, cluster analysis techniques, exploratory data analysis, image segmentation

1. INTRODUCTION

Stroke and cerebrovascular diseases are the third leading cause of mortality in industrial countries after cardiovascular disease and malignancies. Therefore, the analysis of cerebral circulation, became an issue of enormous clinical importance.

In this paper, we present an approach to the analysis of perfusion MRI data that does not imply speculative presumptive knowledge on contrast agent dilution models, but strictly focusses on the observed complete MRI signal time-series. Neural network clustering enables a self-organized data-driven segmentation of dynamic contrast-enhanced perfusion MRI time-series w.r.t. fine-grained differences of signal amplitude and dynamics, such as side asymmetry and local deficits of brain perfusion in patients with stroke, thus providing a useful extension to the computation of conventional perfusion parameter maps. As a result, we obtain both a set of prototypical time-series, representing the temporal information, and a corresponding set of cluster assignment maps, representing the spatial information of the data set. The inspection of these clustering results provides a practical tool for the radiologist to quickly scan the data set for regional differences or abnormalities of brain perfusion.

Independent Component Analyses, Wavelets, Unsupervised Smart Sensors, and Neural Networks III, edited by Harold H. Szu, Proceedings of SPIE Vol. 5818 (SPIE, Bellingham, WA, 2005) · 0277-786X/05/$15 · doi: 10.1117/12.601005

2. EXPLORATORY DATA ANALYSIS METHODS

The following section is dedicated to presenting the algorithms and evaluate the discriminatory power of unsupervised clustering techniques such as "neural gas" network, fuzzy clustering based on deterministic annealing and Kohonen's self–organizing map. These techniques have in common, that they group pixels together based on the similarity of their intensity profile in time (i.e., their time courses).

Let n denote the number of subsequent scans in a perfusion MRI study, and let K be the number of pixels in each scan. The dynamics of each pixel $\mu \in \{1, \ldots, K\}$ can be interpreted as a vector $\mathbf{x}^\mu \in \mathbf{R}^n$ in the n–dimensional feature space of possible signal time–series. In the following the pixel dependent vector $\mathbf{x}^\mu$ will be called a pixel time course (PTC).

Cluster analysis groups image pixels together based on the similarity of their intensity profile in time. Each time course represents one point in a n–dimensional Euclidean space which is subsequently partitioned into clusters, based on the proximity of the input data, during the clustering process.

Here, we employ several vector quantization (VQ) approaches as a method for unsupervised time–series analysis. VQ clustering identifies several groups of pixels with similar PTC, while these groups or clusters are represented by prototypical time–series called codebook vectors (CV) located at the center of their corresponding cluster. The CVs represent prototypical PTCs sharing similar temporal characteristics. Thus, each PTC can be assigned in the crisp clustering scheme to one specific CV according to a minimal distance criterion, while in the fuzzy scheme according to a membership to several CVs. Accordingly, the outcomes of VQ approaches for perfusion MRI data analysis can be plotted as "crisp" or "fuzzy " cluster assignment maps.

VQ approaches determine the cluster centers $\mathbf{w}_i$ by an iterative adaptive update based on the following equation:

$$\mathbf{w}_i(t+1) = \mathbf{w}_i(t) + \epsilon(t) a_i(\mathbf{x}(t), C(t), \kappa)(\mathbf{x}(t) - \mathbf{w}_i(t)) \tag{1}$$

where $\epsilon(t)$ represents the learning parameter, a_i a codebook ($C(t)$) dependent cooperativity function, κ a cooperativity parameter, and $\mathbf{x}$ a randomly chosen feature vector. For perfusion MRI, the feature vector represents the PTC.

The algorithmic description of the "neural gas" network, fuzzy clustering based on deterministic annealing and Kohonen's self–organizing map can be found in[1] and.[2]

3. RESULTS AND DISCUSSION

3.1. Imaging Protocol

Our study group consists of four subjects: (i) two men aged 26 and 37 years without any neurological deficit, history of intracranial abnormality, or previous radiation therapy. They were referred to our department to rule out intracranial abnormality. (ii) two patients (one man and one women aged 61 and 76 years) with subacute stroke (time elapsed since onset of neurological symptoms 2–4 days) who underwent MRI examination as a routine clinical diagnostic procedure. Informed consent was obtained from all subjects after the nature of the study was explained. Dynamic susceptibility contrast-enhanced perfusion weighted MRI was performed on a 1.5 T system (Magnetom Vision, Siemens, Erlangen, Germany) using a standard circularly polarized head coil for radio frequency transmission and detection. First, fluid-attenuated inversion recovery, T2-weighted spin echo, and diffusion weighted MRI sequences were obtained in transversal slice orientation enabling initial localization and evaluation of the cerebrovascular insult in the patients with stroke. Then dynamic contrast-enhanced perfusion weighted MRI was performed using a 2D gradient echo echoplanar imaging (EPI) sequence employing 10 transversal slices with a matrix size of 128×128 pixels, pixel size 1.88×1.88 mm, and a slice thickness of 3.0 mm (TR = 0.8 ms, TE = 0.54 ms, FA = 90°). The dynamic study consisted of 38 scans with an interval of 1.5 s between each scan. The perfusion sequence and an antecubital vein bolus injection (injection flow 3 ml/s) of gadopentetate dimeglumine (0.15 mmol/kg body weight, Magnevist™, Schering, Berlin, Germany) were started simultaneously in order to obtain several (more than six) scans before cerebral first pass of the contrast agent.

3.2. Data Analysis

In an initial presegmentation step, the extracerebral parts of the data set were excluded by definition of a region of interest (ROI). Although automatic presegmentation procedures could be employed, we performed interactive manual contour tracing by a human observer.

For each voxel, the raw gray level time-series $S(\tau)$, $\tau \in \{1, \ldots, 38\}$ was transformed into a PTC of relative signal reduction $x(\tau)$ by

$$x(\tau) = \left(\frac{S(\tau)}{S_0} \right)^{\alpha}, \tag{2}$$

where S_0 denotes the pre-contrast gray level and $\alpha > 0$ a distortion exponent (see below). In our study, S_0 was computed as the average gray level at scan times $\tau \in \{3, 4, 5\}$. The first two scans were discarded from analysis for remaining saturation effects. Different investigations suggest an exponential relationship between the relative signal reduction $x(\tau)$ and the local contrast agent tissue concentration $c(\tau)$[3]:

$$c(\tau) = -\ln x(\tau) = -\alpha \ln \left(\frac{S(\tau)}{S_0} \right), \tag{3}$$

where $\alpha > 0$ is an unknown proportionality constant. Thus, by equation (3), the signal pixel time courses (PTCs) can be transformed into concentration-time curves (CTCs).

Conventional data analysis was performed by computing MTT, relative rCBV, and rCBF parameter maps employing the relations[4]

$$\mathrm{MTT} = \frac{\int \tau \cdot c(\tau)\, d\tau}{\int c(\tau)\, d\tau}, \quad \mathrm{rCBV} = \int c(\tau)\, d\tau, \quad \mathrm{rCBF} = \frac{\mathrm{rCBV}}{\mathrm{MTT}}. \tag{4}$$

For this purpose, contributions of tracer recirculation were eliminated by fitting a gamma variate function to the measured concentration-time curves $c(\tau)$ using the Marquardt algorithm for nonlinear least-squares estimation. For conceptual difficulties with regard to perfusion parameter computation according to equations (4), we refer to the literature.[5]

Self-controlled hierarchical neural network clustering of PTCs $x(\tau)$ was performed by fuzzy clustering based on deterministic annealing employing 16 CVs, i.e. a maximal number of 16 separate clusters at the end of the hierarchical VQ procedure. We use a batch Expectation Maximization (EM) version of fuzzy clustering based on deterministic annealing in which the computation of CVs $\mathbf{w}_j$ (M-step) and assignment probabilities a_j (E-step) is decoupled and iterated until convergence at each annealing step characterized by a given 'temperature' $T = 2\rho^2$. Clustering was performed employing 200 annealing steps corresponding to approx. 8×10^3 EM iterations within an exponential annealing schedule for ρ. Codebook control parameters like load balance deviation, center of mass shift, entropy, and reconstruction error were computed for each annealing step. The constant α in equation (2) was chosen to $\alpha = 3$.

Besides fuzzy clustering based on deterministic annealing, we performed alternative neural network clustering procedures on our data: SOM clustering and k-means type (fuzzy c-means) VQ. In addition, exploratory analyses on subsets of the data were done with regard to the following modifications: (i) Different number of CVs: 16, 25, 36, 49, and 81 CVs were tested. (ii) Different number of annealing steps: 36, 64, 128, and 200 annealing steps were tested corresponding to approx. $5 \times 10^2 - 8 \times 10^3$ EM iterations. (iii) Different preprocessing strategies: α was varied within the interval $\alpha \in [0.1, 10]$. Clustering of raw gray level time-series ($S(\tau)$), of normalized and non-normalized gray level differences ($S(\tau) - S_0$), and of normalized and non-normalized concentration-time curves ($c(\tau)$) was performed. (iv) Different levels of information extraction from PTCs: Besides neural network analysis of time-series (see (iii)), additional exploratory cluster analysis was performed in the two-dimensional feature space of blood flow parameter vectors (MTT, rCBF), and the three-dimensional feature space of gamma variate fit parameters.

Clustering results were evaluated by (i) assessment of cluster assignment maps, i.e. cluster membership maps according to a minimal distance criterion in the metric of the PTC feature space, (ii) qualitative visual analysis

of corresponding cluster-specific concentration-time curves (CTCs), (iii) quantitative analysis of cluster-specific CTCs by computing cluster-specific relative perfusion parameters (rCBV, rCBF, MTT), (iv) comparison of cluster assignment maps with conventional pixel-specific relative perfusion parameter maps, (v) analysis of clustering results in two-dimensional perfusion parameter plots, (vi) quantitative assessment of asymmetry between the affected and a corresponding non-affected contralateral brain region based on clustering results in patients with stroke.

3.3. Evaluation

Clustering results for a 38 scan dynamic contrast-enhanced MRI perfusion study of a patient with a subacute stroke affecting the right basal ganglia are presented in figs. 1 and 2. After discarding the first two scans, a relative signal reduction time-series $x(\tau), \tau \in \{1, \ldots, n\}, n = 36$ can be computed for each voxel according to equation (2). Clustering these PTCs identifies groups of pixels with similar signal dynamics. Fig. 1 shows the 'cluster assignment maps' overlaid onto an EPI scan of the perfusion sequence. In these maps, all the pixels are highlighted that belong to a specific cluster. The decision on assigning a pixel ν characterized by the PTC $\vec{x}_\nu = (x_\nu(\tau)), \tau \in \{1, \ldots, n\}$ to a specific cluster j is based on a minimal distance criterion in the n-dimensional time-series feature space, i.e. ν is assigned to cluster j, if the distance $\|\vec{x}_\nu - \vec{w}_j\|$ is minimal, where $\vec{w}_j$ denotes the CV belonging to cluster j. Each CV can be interpreted as the weighted centroid of all the PTCs belonging to this cluster.

Fig. 2 shows the prototypical cluster-specific concentration-time curves (CTCs) belonging to the pixel clusters of fig. 1. These can be computed from equation (3), where the pixel-specific PTC $x(\tau)$ is replaced by the cluster-specific CV.

The region of the cerebrovascular insult in the right basal ganglia is clearly depicted by cluster #7. Note the small corresponding CTC amplitude, i.e. the small cluster-specific rCBV, rCBF as well as the large MTT. Cluster #3 contains peripheral and adjacent regions. Clusters #12, #14 represent larger vessels located in the sulci. Note the large amplitudes and apparent recirculation peaks in the corresponding cluster-specific CTCs in fig. 2.

Clusters #2, #12, and #11 may be attributed to large, intermediate and small parenchymal vessels of the non-affected left side represented by subsequently increasing MTT, decreasing rCBF, rCBV, and smaller recirculation peaks. The procedure is even able to depict subtle differences of contrast agent first-pass times: Note the ability to distinguish between left and right side perfusion as indicated by minimal time-to-peak differences of clusters #12 and #14. Pixels representing regions supplied by a common arterial input tend to be collected into separate clusters: For example, clusters #6 and #11 contain many pixels that can be attributed to the supply region of the left middle cerebral artery, whereas clusters #3 and #4 include regions supplied by the right middle cerebral artery. Note the differences with regard to cluster-specific MTT, rCBF, and rCBV between corresponding contralateral clusters #6 vs. #3 as well as #4 vs. #11 indicating an apparent perfusion deficit at the expense of the right-hand side.

The structural lesion in the region of the right basal ganglia is indicated by the diffusion weighted image fig. 3a. Figs. 3b, c, and d show conventional pixel-based MTT, rCBF, and rCBV maps at an equivalent slice position. Note that the clustering results in figs. 1 and 2 are in good agreement with the findings of these parameter maps, however, as shown above, clustering enables a more detailed analysis of spatiotemporal perfusion properties by self-organized grouping of pixels with similar signal dynamics.

Fig. 4 shows a quantitative analysis of clustering results with regard to side differences of brain perfusion. The best-matching cluster #7 representing the infarct region in fig. 1 is plotted in fig. 4a. In order to enable quantitative analysis of perfusion asymmetry between the affected and the non-affected side, a spatially contiguous region is constructed by spatial low-pass filtering and thresholding this pixel cluster. Note that this is not an integral part of the clustering procedure: it only serves as an instrument to exclude isolated pixels in this example, i.e. to define a circumscript ROI that can be derived from the clustering results in a well-defined manner. The resulting ROI is plotted in fig. 4b (white region). Now, a symmetrical ROI can be defined at an equivalent contralateral position (light gray region). Finally, the average CTCs of all the pixels in the ROIs are computed and visualized in the lower line of fig. 4 along with the corresponding quantitative perfusion parameters: Note the apparent

difference between the affected (fig. 4c) and the non-affected (fig. 4d) side with regard to CTC amplitude and dynamics, as indicated by highly differing corresponding quantitative perfusion parameters as well.

For comparison, clustering results for a perfusion study in a control subject without evidence of cerebrovascular disease are presented in figs. 5 and 6. Clusters #1, #4, and #15 may be attributed to larger vessels primarily located in the cerebral sulci, whereas most of the other clusters seem to represent parenchymal vascularization. Note that, in contrast to the results of the stroke patient data in figs. 1, 2, 3, and 4, there is no evidence of side-asymmetry with regard to both the temporal pattern and the amplitude of brain perfusion. This is expressed by the observation that, in contrast to fig. 1, each cluster contains pixels in roughly symmetrical regions of both hemispheres. Furthermore, there is no cluster indicating a localized perfusion deficit.

3.4. ROC Analysis

It is important to perform a quantitative analysis of the relative performance of the introduced cluster analysis techniques. For the dynamic perfusion MRI data, a comparative quantitative evaluation is done among the four clustering techniques, "neural gas" network (NG), Kohonen's self–organizing map (SOM), fuzzy clustering based on deterministic annealing (MFE), and fuzzy c–means vector quantization. For the fuzzy c–means vector quantization we employ two different implementations: fuzzy c–means with unsupervised codebook initialization (FSM), and the fuzzy c–means algorithm (FVQ) with random codebook initialization. We analyzed the classification outcome for four subjects: subject 1 (stroke in the right basal ganglia), subject 2 (large stroke in the supply region of the middle cerebral artery), and subject 3 and 4 (both with no evidence of cerebrovascular disease). To do so, we compared the proposed algorithms for 3 up to 36 codebook vectors in terms of ROC analysis using two different performance metrics. The first is based on the classification outcome regarding the discrimination of the concentration–time curves based on the rCBV–value. The second paradigm represents the discrimination capability of the codebook vectors based on their MTT–value. We report the ROC performances for the four subjects in Figure 7. The Figure illustrates the average area under the curve and its deviations for 20 different ROC runs using the same parameters but different algorithms' initializations. From this Figure, we can see that based on clustering we obtain a good distinction between the concentration–time curves based on their rCBV–values. Also, the MTT–values play a secondary role in the clustering of time series, as it can be seen from the area under the curves.

In general, the larger the number of the codebook vectors the higher is the area under the curve for the subjects 1,3, and 4. Subject 2 shows exactly the opposite effect: very good classification results are obtained even for a low codebook vector number. A possible explanation of this aspect is because of the large extent of the infarct area. Also, for the patients without evidence of a cerebrovascular disease the area under the ROC–curve is smaller than that for the patients with stroke.

4. CONCLUSION

In the present paper, we have experimentally compared four different unsupervised clustering techniques as a tool for the analysis of dynamic cerebral contrast–enhanced perfusion MRI time–series.

The goal of the paper was to determine the robustness and reliability of clustering methods in providing a self–organized segmentation of perfusion MRI data sharing common properties of signal dynamics. By using the whole information provided by the dynamic time–series, we introduce an extension to the conventional method of analyzing perfusion MRI studies based on the evaluation of a few parameters such as MTT, rCBV, and rCBF.

In contrast to the conventional extraction of perfusion parameters alone, neural network clustering

(i) does not discard information contained in the signal dynamics of MRI time-series

(ii) its interpretation is not biased by the indicator-dilution theory of non-diffusible tracers, the applicability of which is questionable under pathological conditions of a disrupted blood-brain barrier.

However, clustering results may be interpreted in the light of the indicator-dilution theory as well, as conventional perfusion parameters like MTT, rCBV, and rCBF values can be computed from the resulting prototypical cluster-specific CTCs.

The proposed clustering techniques were able to unveil regional differences of brain perfusion characterized by subtle differences of signal amplitude and dynamics. They could provide a rough segmentation with regard to vessel size, detect side asymmetries of contrast-agent first pass, and identify regions of perfusion deficit in patients with stroke.

The performed ROC–analysis shows that the rCBV represents a good performance metrics for the classification of the pixel time courses while MTT plays only a secondary role.

Our study shows that unsupervised clustering results are in good agreement with the information obtained from conventional perfusion parameter maps, but may sometimes unveil additional hidden information e.g. detect subtle side asymmetries of brain perfusion or disentangle signals with regard to different vessel sizes. In this sense, clustering is not a competitive, but a complementary additional method that may extend the information extracted from conventional perfusion parameter maps by taking into account fine-grained differences of MRI signal dynamics in perfusion studies. It provides computer–aided support to appropriate data processing in order to assist the neuroradiolgist, and not to replace his interpretation.

REFERENCES

1. A. Wismüller, A. Meyer-Bäse, O. Lange, and D. Auer, "Comparison of two exploratory data analysis methods for fmri: Unsupervised clustering vs. independent component analysis," *Invited Paper, Proceedings of SPIE, Vol. 5103* , pp. 104–115, 4 2004.
2. A. Meyer-Bäse, *Pattern Recognition for Medical Imaging*, Elsevier Science/Academic Press, 2003.
3. B. Rosen, J. Belliveau, J. Vevea, and T. Brady, "Perfusion imaging with NMR contrast agents," *Magnetic Resonance in Medicine* **14**, pp. 249–265, 10 1990.
4. L. Axel, "Cerebral blood flow determination by rapid-sequence computed tomography," *Radiology* **137**, pp. 679–686, 10 1980.
5. R. Weisskoff, D. Chesler, J. Boxerman, and B. Rosen, "Pitfalls in MR measurement of tissue blood flow with intravascular tracers: which mean transit time?," *Magnetic Resonance in Medicine* **29**, pp. 553–559, 10 1993.

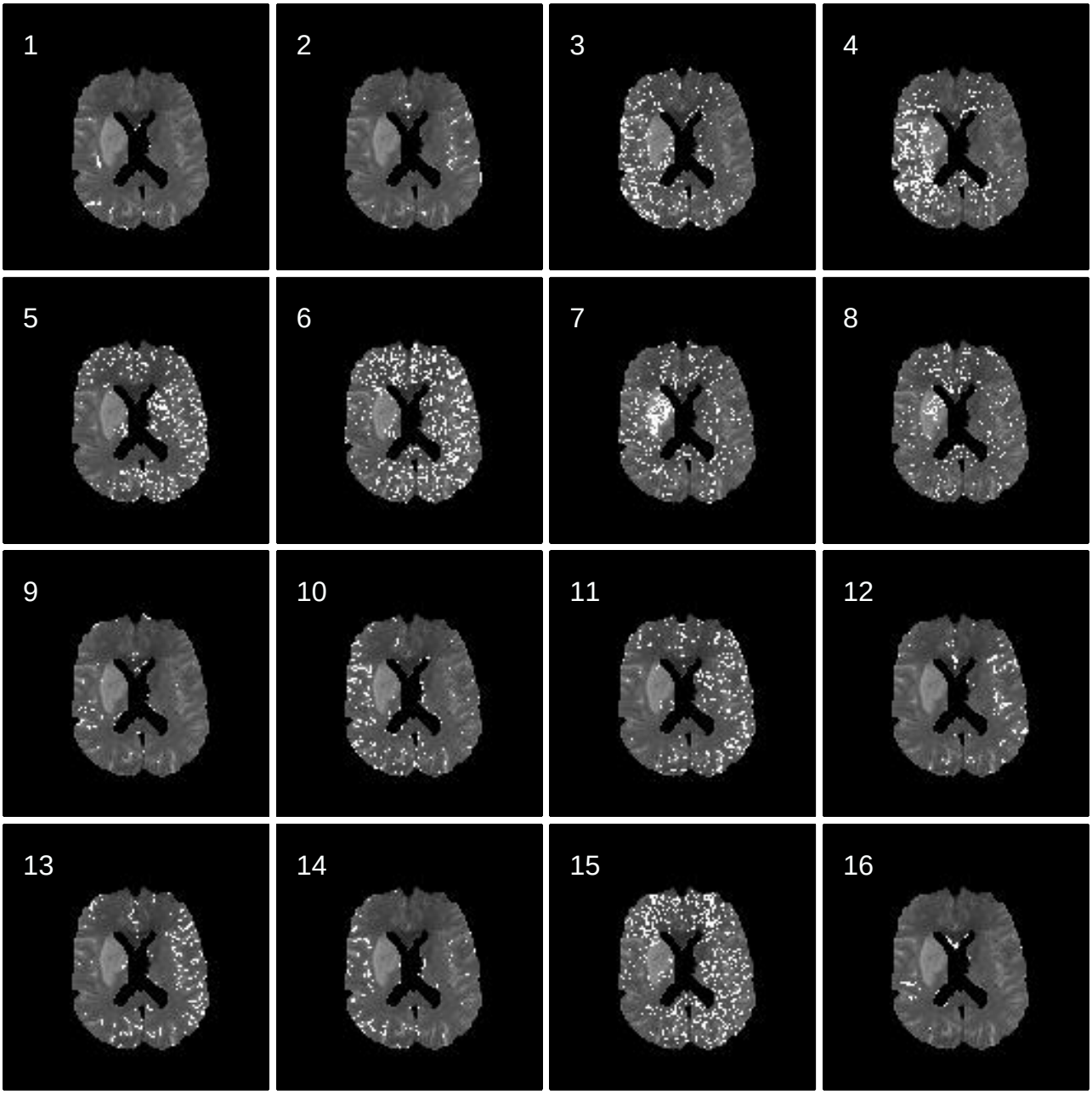

Figure 1. Cluster assignment maps for "neural gas" network of a dynamic perfusion MRI study in a patient with stroke in the right basal ganglia.

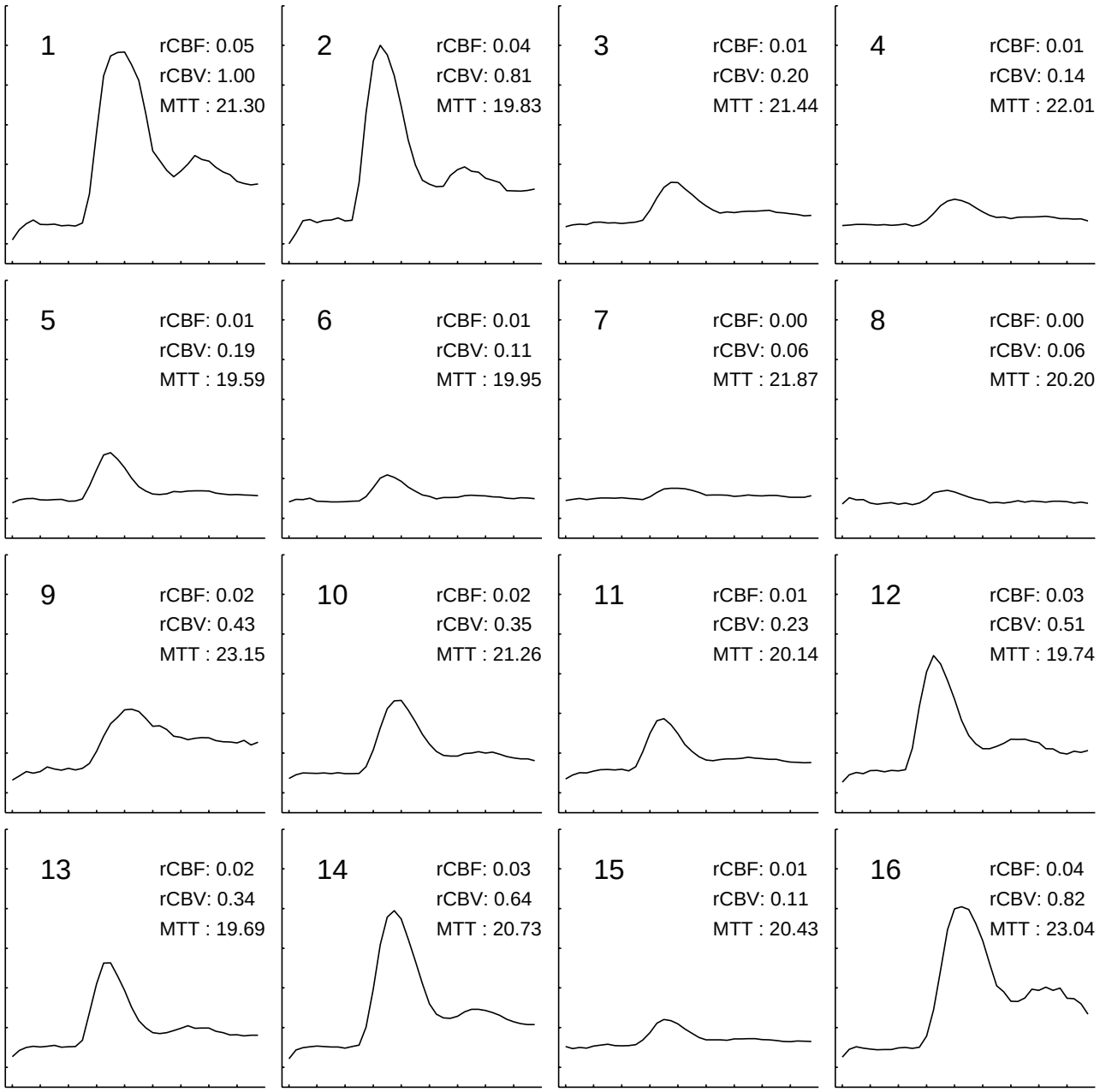

Figure 2. Cluster-specific concentration-time curves for "neural gas" network of a dynamic perfusion MRI study in a patient with stroke in the right basal ganglia. Cluster numbers correspond to fig. 1. MTT values are indicated as multiples of the scan interval (1.5 s), rCBV values are normalized w.r.t. the maximal value (cluster #9). rCBF values are computed from MTT and rCBV by equation (4).

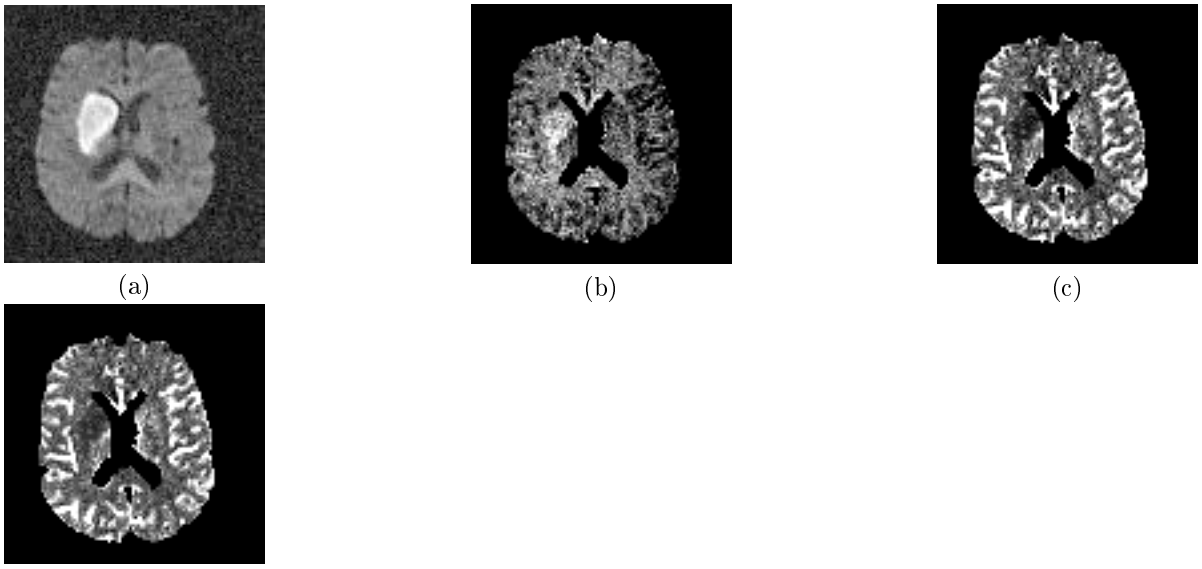

(a) (b) (c) (d)

Figure 3. Diffusion weighted MR image and conventional perfusion parameter maps of the same patient as in figs. 1 and 2. (a) Diffusion weighted MR image, (b) MTT map, (c) rCBV map, (d) rCBF map.

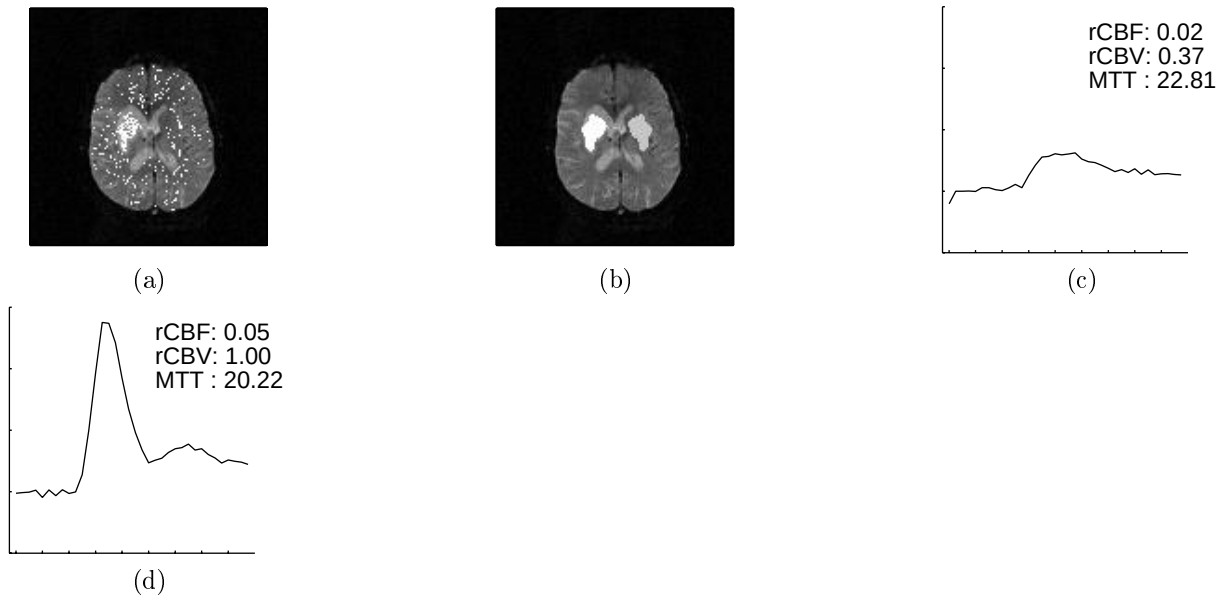

(a) (b) (c) (d)

Figure 4. Quantitative analysis of the results for "neural gas" network in fig. 1 with regard to side asymmetry of brain perfusion. (a) Best-matching cluster of fig. 1 representing the infarct region , (b) contiguous ROI constructed from (a) by spatial low-pass filtering and thresholding (white) and a symmetrical ROI at an equivalent contralateral position (light gray), (c) average concentration-time curve of the pixels in the ROI of the affected side, (d) average concentration-time curve of the pixels in the ROI of the non-affected side.

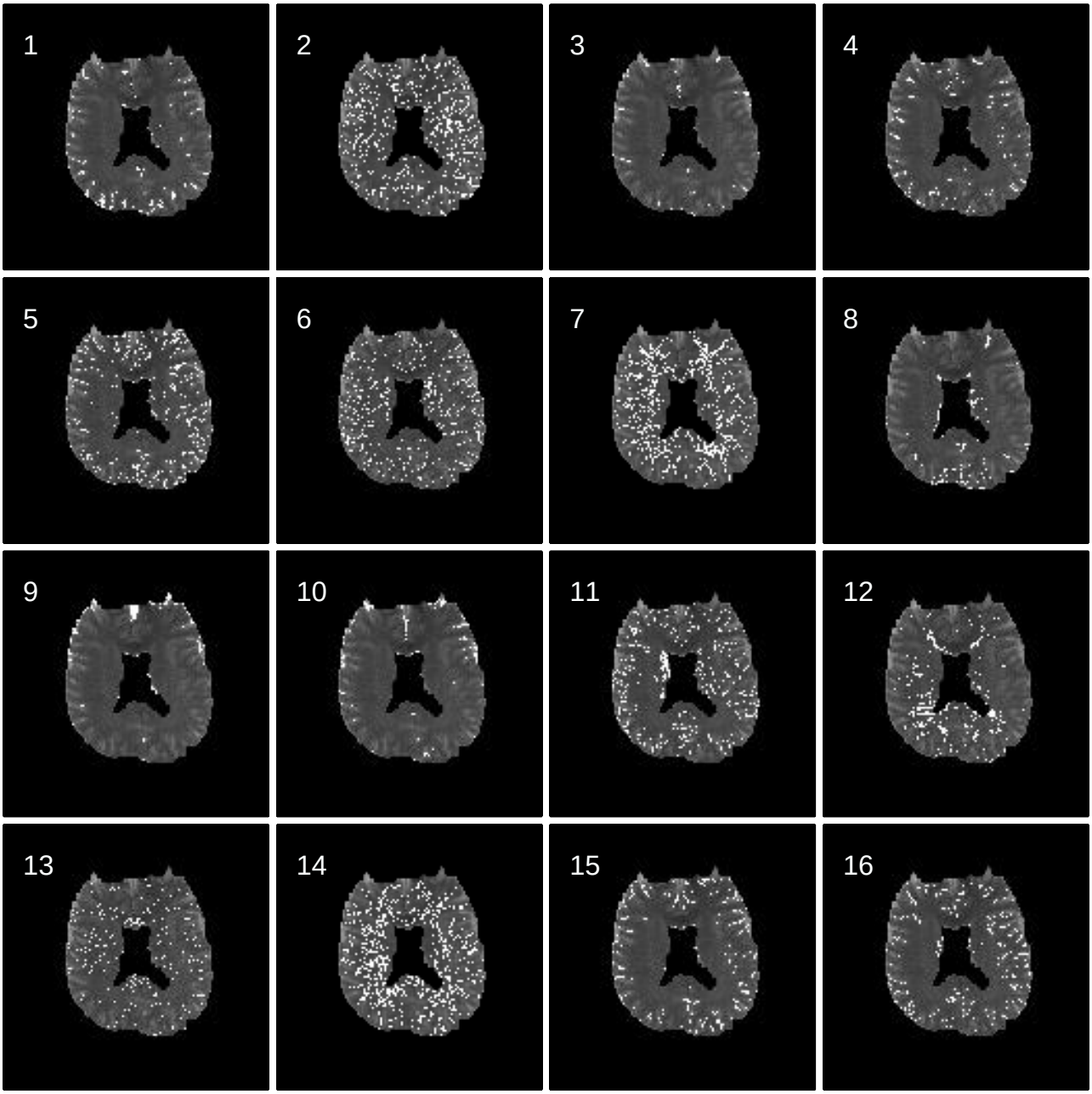

Figure 5. Cluster assignment maps for "neural gas" network of a dynamic perfusion MRI study in a control subject without evidence of cerebrovascular disease.

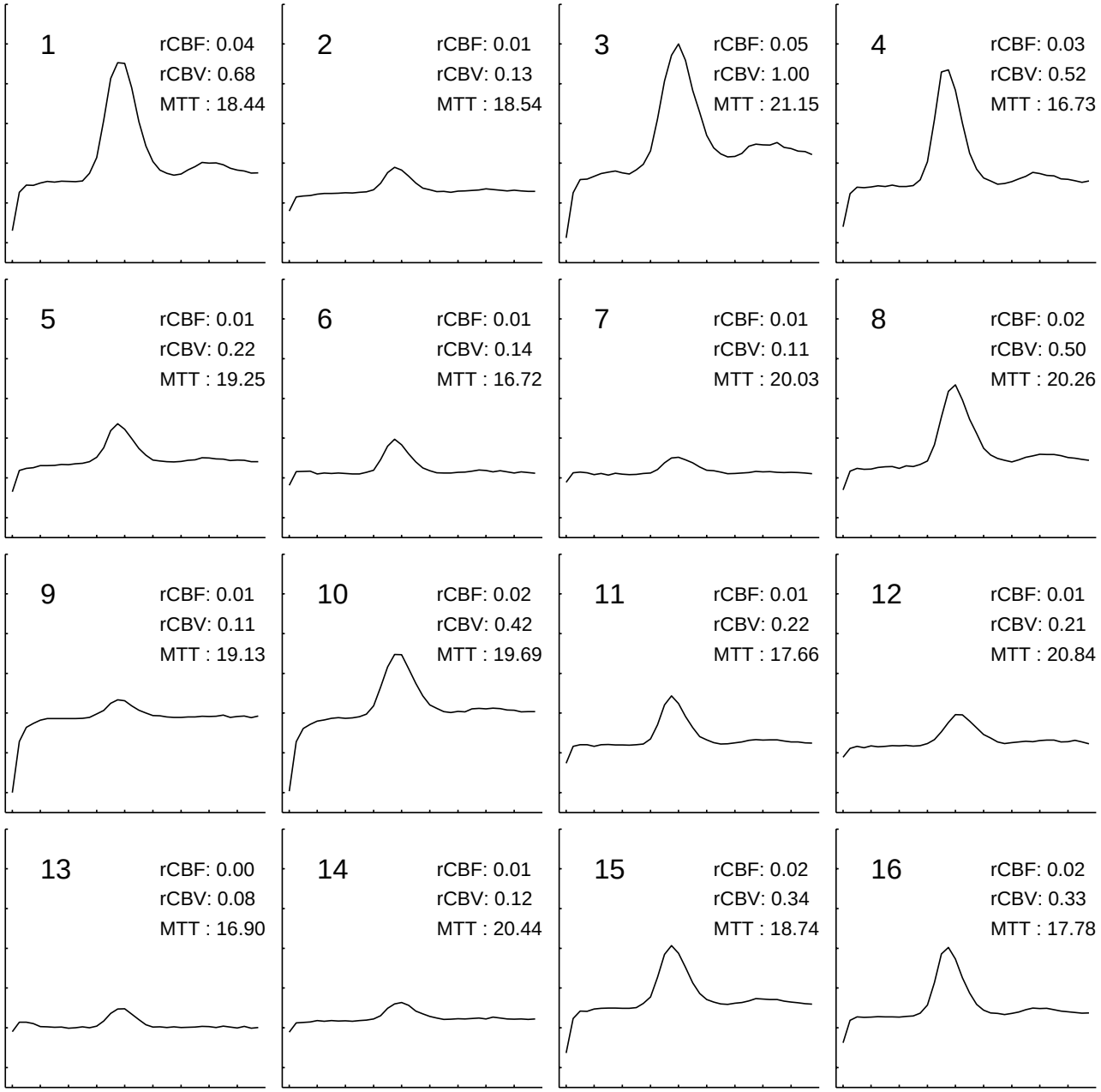

Figure 6. Cluster-specific concentration-time curves for "neural gas" network of a dynamic perfusion MRI study in a control subject without evidence of cerebrovascular disease. Cluster numbers correspond to fig. 5.

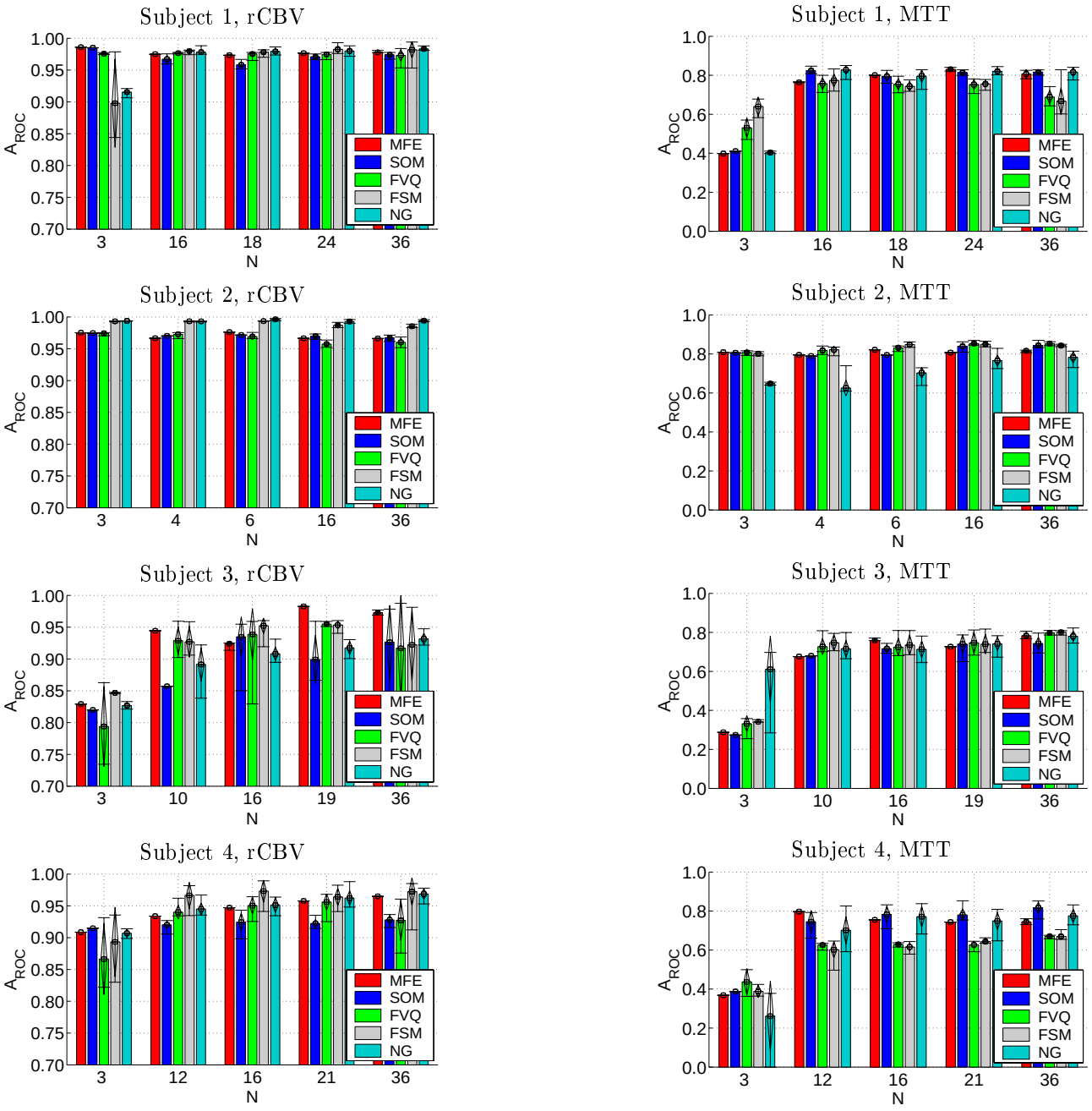

Figure 7. Results of the comparison between the different clustering analysis methods on perfusion MRI data. These methods are: Kohonen's map (SOM), "neural gas" network, fuzzy clustering based on deterministic annealing, fuzzy c–means with unsupervised codebook initialization (FSM), fuzzy c–means algorithm (FVQ) with random codebook initialization, and the "neural gas" network. It is illustrated the average area under the curve and its deviations for 20 different ROC runs using the same parameters but different algorithms' initializations. The number of chosen codebook vectors for all techniques is between 3 and 36 and results are plotted for four subjects. Subject 1 and 2 had a subacute stroke, while subject 3 and 4 gave no evidence of a cerebrovascular disease. The ROC–analysis is based on two performance metrics: regional cerebral blood volume (rCBV) (left column) and mean transit time (MTT) (right column).